Rho-mDia1 pathway is required for adhesion, migration, and T-cell stimulation in dendritic cells

Hideaki Tanizaki,[1] Gyohei Egawa,[1,2] Kayo Inaba,[3] Tetsuya Honda,[1] Saeko Nakajima,[1] Catharina Sagita Moniaga,[1] Atsushi Otsuka,[1] Toshimasa Ishizaki,[4] Michio Tomura,[5] Takeshi Watanabe,[2] Yoshiki Miyachi,[1] Shuh Narumiya,[4] Takaharu Okada,[6] and Kenji Kabashima[1,2]

[1]Department of Dermatology and [2]Center for Innovation in Immunoregulative Technology and Therapeutics, Kyoto University Graduate School of Medicine, Kyoto, Japan; [3]Department of Animal Development and Physiology, Kyoto University Graduate School of Biostudies, Kyoto, Japan; [4]Department of Pharmacology, Kyoto University Graduate School of Medicine, Kyoto, Japan; and [5]Laboratory for Autoimmune Regulation and [6]Research Unit for Immunodynamics, Research Center for Allergy & Immunology, RIKEN, Yokohama, Japan

Dendritic cells (DCs) are essential for the initiation of acquired immune responses through antigen acquisition, migration, maturation, and T-cell stimulation. One of the critical mechanisms in this response is the process actin nucleation and polymerization, which is mediated by several groups of proteins, including mammalian Diaphanous-related formins (mDia). However, the role of mDia in DCs remains unknown. Herein, we examined the role of mDia1 (one of the isoforms of mDia) in DCs. Although the proliferation and maturation of bone marrow-derived DCs were comparable between control C57BL/6 and mDia1-deficient (mDia1$^{-/-}$) mice, adhesion and spreading to cellular matrix were impaired in mDia1$^{-/-}$ bone marrow–derived DCs. In addition, fluorescein isothiocyanate-induced cutaneous DC migration to draining lymph nodes in vivo and invasive migration and directional migration to CCL21 in vitro were suppressed in mDia1$^{-/-}$ DCs. Moreover, sustained T-cell interaction and T-cell stimulation in lymph nodes were impaired by mDia1 deficiency. Consistent with this, the DC-dependent delayed hypersensitivity response was attenuated by mDia1-deficient DCs. These results suggest that actin polymerization, which is mediated by mDia1, is essential for several aspects of DC-initiated acquired immune responses. (*Blood*. 2010;116(26):5875-5884)

Introduction

When external antigens invade the body, professional antigen-presenting dendritic cells (DCs) capture them, up-regulate the expression levels of costimulatory molecules and chemokine receptors such as CCR7 and CXCR4, and migrate to draining lymphoid tissues via the lymphatic vessels.[1-4] During the initial phase of T-cell priming within the T-cell areas of lymph nodes (LNs), DCs project polarized membrane extensions that facilitate repeated and, under certain conditions, sustained DC-T cell contacts called immunologic synapses, which facilitate T-cell proliferation and differentiation.[5]

The actin cytoskeleton undergoes continuous remodeling and serves as the machinery for antigen acquisition, cell migration, and sustained cell contact.[6-8] A critical step in this remodeling process is the formation of actin oligomers, which serve as nuclei for further polymerization. Actin nucleation and polymerization in mammalian cells are catalyzed by several groups of proteins. Two of the most important catalyst groups here are the mammalian Diaphanous-related (mDia) formins, which produce long and straight actin filaments, and the Wiskott-Aldrich syndrome protein (WASP)–Arp2/3 system, which produces a branched actin meshwork.[9] Lack of WASP expression results in defects in T-cell proliferation, T-cell receptor capping, phagocytosis of macrophages, and migration of immune cells,[10] all of which are involved in chemotaxis, chemokinesis, and adhesion.[11]

The mDia family formins are among the effectors of Rho GTPase. The family is composed of 3 isoforms: mDia1, mDia2, and mDia3. The ability of mDia proteins to promote rapid assembly of actin filaments appears to be crucial to cell polarity, morphogenesis, and cytokinesis.[12-15] Most studies on the mDia family have used cultured cells.[9] As a result, the roles of mDia proteins in vivo remain unclear. Recently, we and other researchers have generated mice deficient in mDia1 and reported on its role in T-cell proliferation, trafficking, and interaction with DCs.[16,17]

Because the mDia family drives actin polymerization, mDia proteins may contribute to the functions of DCs,[18] but the roles of mDia in DCs are still unclear. In this study, we studied mDia1-deficient (mDia1$^{-/-}$) mice and the cells derived from these mice, and found that mDia1 in DCs is essential for adhesion to fibronectin, transmigration through small pore membranes, directional migration, and sustained interaction with T cells.

Methods

Mice, reagents, flow cytometry, and cell sorting

We generated mDia1$^{-/-}$ mice[16] and backcrossed them for more than 10 generations onto C57BL/6J Slc (B6) mice (Japan SLC Inc). OT-I, OT-II (The Jackson Laboratory), and BALB/c (Japan SLC Inc) mice were bred at the Institute of Laboratory Animals at Kyoto University on a 12-hour

Submitted January 12, 2010; accepted September 15, 2010. Prepublished online as *Blood* First Edition paper, September 29, 2010; DOI 10.1182/blood-2010-01-264150.

The online version of this article contains a data supplement.

The publication costs of this article were defrayed in part by page charge payment. Therefore, and solely to indicate this fact, this article is hereby marked "advertisement" in accordance with 18 USC section 1734.

light/dark cycle under specific pathogen–free conditions. Eight- to 10-week-old female mice were used for all experiments. All experimental procedures were approved by the Institutional Animal Care and Use Committee of Kyoto University Graduate School of Medicine.

Carboxyfluorescein succinimidyl ester (CFSE) and CellTracker Red CMTPX were purchased from Invitrogen. Fluorescein isothiocyanate (FITC), phycoerythrin (PE), PE-Cy5, PE-Cy7, allophycocyanin, Pacific Blue–conjugated RM4-5 (anti-CD4), 53-6.7 (anti-CD8), HI111 (anti-CD11a), M1/70 (anti-CD11b), HL3 (anti-CD11c), HM40-3 (anti-CD40), YN1/1.7.4 (anti-CD54), Ly-22 (anti-CD62L), 16-10A1 (anti-CD80), 24-31 (anti-OX40L), GL1 (anti-CD86), M5/114.15.2 (anti–major histocompatibility complex [MHC] class II), 4B12 (anti-CCR7) monoclonal antibodies (Abs), and PE-Cy7–conjugated streptavidin were purchased from eBioscience. Biotin-conjugated eBioRMUL2 (anti-Langerin) and PECy-7–conjugated H1.2F3 (anti-CD69) Abs were purchased from BD Biosciences. Flow cytometry was performed using FACSCanto II (BD Biosciences) and analyzed with FlowJo Version 8.8.7 software (TreeStar). Cell sorting was performed using an autoMACS system (Miltenyi Biotec) or a cell sorter (FACSAria II, BD Biosciences).[19]

Cell culture, MLR, and enzyme-linked immunosorbent assay

The complete RPMI (cRPMI) culture medium consisting of RPMI 1640 (Sigma-Aldrich) containing 10% heat-inactivated fetal calf serum, 5×10^{-5}M 2-mercaptoethanol, 2mM L-glutamine, 25mM N-2-hydroxyethylpiperazine-N′-2-ethanesulfonic acid, 1mM nonessential amino acids, 1mM sodium pyruvate, 100 units/mL penicillin, and 100 μg/mL streptomycin, was used, unless otherwise indicated.

For bone marrow–derived DC (BMDC) culture, 5×10^6 BM cells were cultured in 10 mL of cRPMI supplemented with 5 ng/mL recombinant murine granulocyte-macrophage colony-stimulating factor (PeproTech) for 5 to 7 days.[20]

For spleen cell suspensions, spleens were cut into small pieces and digested by being mixed for 25 minutes at 37°C with RPMI 1640 containing 1.6 mg/mL type II collagenase (Worthington Biochemical) and 100 μg/mL DNase I (Sigma-Aldrich).

For epidermal cell suspensions, ear skin sheets were floated on 0.25% trypsin in phosphate-buffered saline (PBS) for 30 minutes at 37°C.[21] The epidermis was separated from the dermis with forceps in PBS supplemented with 10% fetal calf serum. The epidermis was filtered through a 40-μm cell strainer. For dermal cell suspensions, the dermis was further digested with 1.6 mg/mL type II collagenase and 100 μg/mL DNase I in cRPMI for 25 minutes at 37°C. The cells were then filtered through a 40-μm cell strainer.

For allogeneic mixed lymphocyte reaction (MLR), 1×10^3 or 10^4 BMDCs with a B6 background were pretreated with mitomycin C and incubated with 5×10^5 $CD4^+$ T cells from BALB/c mice in 200 μL of cRPMI for 3 days. The cells were pulsed with 0.5 μCi ^{3}H-thymidine for the last 24 hours and subjected to liquid scintillation counting. For the measurement of cytokine production, culture supernatants were collected 72 hours after the start of cultivation and measured with an enzyme-linked immunosorbent assay kit (BD Biosciences).

Chemotaxis, TAXIScan, adhesion, cell polarity, and FITC-induced DC migration assays

For the chemotaxis assay, suspensions of epidermal cells were prepared and incubated overnight, then 1×10^6 cells were transferred into the upper chamber of the transwell with 3- or 8-μm pore size filters (BD Biosciences), and 10 or 100 ng/mL of CCL21 (R&D Systems) was added to the lower chamber and allowed to incubate for 3 hours or 24 hours at 37°C. The cells that migrated to the lower chambers were stained with MHC class II and counted by flow cytometry. The migration index was presented as a percentage of input: the number of cells in each lower chamber was divided by the total number of cells placed in the corresponding upper chamber.

For the evaluation of invasive migration, the upper chambers (8-μm pore size) were coated with Matrigel (BD Biosciences), which consists of laminin, collagen IV, heparin sulfate proteoglycans, and entactin/nidogen. After 24 hours of incubation, the upper chambers were washed 3 times with 500 μL of PBS. The upper chambers were treated with 500 μL of dispase (0.15 mg/mL; Invitrogen), cRPMI for 60 minutes at 37°C to collect the cells in the Matrigel.

For the TAXIScan assay, time-lapse images of BMDCs during chemotaxis were obtained using TAXIScan (GE Healthcare) as described previously.[22] First, 2×10^6 BMDCs were applied to the lower side of the chamber. Data were collected at 60-second intervals for 6 hours, starting at 10 minutes after addition of 1 μL of CCL21 (10 μg/mL) to the upper side of the chamber, and analyzed with the TAXIScan Analyzer 2 (GE Healthcare).

For the adhesion assay, 4×10^4 CFSE-labeled BMDCs were incubated in a 96-well plate that had previously been coated overnight with PBS with or without 10 μg/mL of fibronectin (FN), and incubated for 45 minutes at 37°C. The plate was read in a fluorescent plate reader (Wallac 1420 ARVOsx, PerkinElmer Life and Analytical Sciences) at 485-nm excitation and 535-nm emission, both immediately after incubation, to determine the original number of cells (the fluorescent total). The plate was read again after it had been washed twice by vigorous pipetting with 200 μL of PBS and decanting, to determine the number of cells that had adhered (the fluorescent adhesion). The percentage of adherence was calculated as the ratio of fluorescent adhesion/fluorescent total.

To evaluate the cell polarity induced by the chemokine gradient, 25 μL of CCL21 (10 ng/mL) was added to the edge of the BMDC culture in 24-well plates. Thirty minutes later, the culture medium was washed out, and the cells were fixed, permeabilized, and stained with phalloidin.

For FITC-induced cutaneous DC migration, the footpads of mice were painted with 50 μL of 2% FITC (Sigma-Aldrich), dissolved in a 1:1 (vol/vol) acetone/dibutyl phthalate (Sigma-Aldrich) mixture; 72 hours later, the number of cutaneous DCs that had migrated into skin-draining popliteal and inguinal LNs was counted by flow cytometry.

Immunostaining

BMDCs were plated on coverslips coated with or without 10 μg/mL FN for 16 hours. The cells were fixed for 15 minutes with 3.7% formalin (Wako) and permeabilized with 0.1% Triton-X (Sigma-Aldrich) in PBS for 7 minutes at room temperature. Next, slides were incubated with the anti-mDia1 or anti-vinculin Ab (BD Biosciences) and Alexa Fluor 488–conjugated phalloidin (Invitrogen) at room temperature for 1 hour, then stained with Alexa Fluor 546–conjugated goat anti–mouse IgG (Invitrogen) for 30 minutes at room temperature. The slides were mounted in ProLong Gold Antifade reagent (Invitrogen), and fluorescence images were obtained using a BIOREVO BZ-9000 system (Keyence).

Antigen acquisition, DC kinetics, T-cell priming, and DTH model

The activity of antigen acquisition by DCs was measured with 2 mg/mL FITC-ovalbumin (OVA; Invitrogen). After incubation for 45 minutes at 4°C or 37°C, the cells were washed 4 times with PBS and the mean fluorescence intensity of FITC was measured by flow cytometry.[22]

For the evaluation of the kinetics of DCs in the LNs, BMDCs were cultured for 7 days, stimulated with 200 ng/mL of lipopolysaccharide (LPS) for 2 hours, and labeled with 5μM CFSE or 3.3μM CMTPX at 37°C for 20 minutes.

For the assessment of the interaction between $CD4^+$ T cells and BMDCs, BMDCs were cultured for 7 days, pulsed with 1 μg/mL of OVA (Sigma-Aldrich) for 30 minutes at 37°C, stimulated with 200 ng/mL of LPS for 2 hours, and labeled with 5μM CFSE at 37°C for 20 minutes. A total of 3 million B6 or $mDia1^{-/-}$ BMDCs were injected into the footpads of B6 mice. Twenty-four hours later, $CD4^+$ T cells from OT-II mice purified with $CD4^+$ T cell–negative separation kits (Miltenyi Biotec) were labeled with 3.3μM CMTPX and transferred into B6 mice intravenously (1×10^7 cells per mouse). Two hours later, the popliteal and inguinal LNs were harvested and observed for 90 minutes under 2-photon microscopy to measure the period of conjugate formation between T cells and DCs.

For assessing the ability of DCs to induce OT-II $CD4^+$ T-cell proliferation or OT-I $CD8^+$ T-cell proliferation, 20 μL of 0.5 μg/mL OVA emulsified with complete Freund adjuvant (CFA; Difco) and PBS (1:1) was injected into mouse footpads. $CD4^+$ T cells from OT-II mice and $CD8^+$ T cells from OT-I mice were isolated using magnetic bead separation

(Miltenyi Biotec) and labeled with 8μM CFSE. One day after injection of OVA-CFA emulsion, 1×10^7 CFSE-labeled OT-II $CD4^+$ T cells or OT-I $CD8^+$ T cells were transferred via the tail vein. After 48 hours, draining popliteal and inguinal LNs and nondraining axillary LNs were collected and analyzed by flow cytometry.

For delayed-type hypersensitivity (DTH) response, mice were sensitized with 20 μL of 0.5 mg/mL OVA in CFA or with 5×10^5 LPS-pretreated and 1-μg/mL-OVA-pulsed BMDCs in 20 μL PBS subcutaneously injected into the front footpads. Five days later, the mice were challenged with an injection of 20 μL of 0.5 mg/mL OVA in CFA into the hind footpads. Footpad swelling was measured before and 48 hours after the challenge. Controls consisted of CFA injections containing no OVA or sensitization with non–OVA-pulsed DCs.

Two-photon imaging

Two-photon imaging was performed as previously described[23] with some modifications. Briefly, we used a custom-built, video-rate multiphoton microscope: an upright BX61WI microscope (Olympus) fitted with a ×20 water-immersion objective lens (numerical aperture, 0.95), a Spectra-Physics Mai Tai femtosecond laser (Newport), and a resonant-mirror scan head. The image acquisition process, the z-axis stepper, shutters, and the emission filter wheel were under software control (FluoView10-ASW1.6, Olympus). LNs were cemented to the base of the imaging chamber with a thin film of veterinary-grade superglue and were continuously superperfused with warm (35°-37°C) RPMI 1640 medium bubbled with 95% O_2/5% CO_2.

Quantitative reverse-transcribed polymerase chain reaction analysis

Total RNA was isolated using an RNeasy kit (QIAGEN) with an on-column DNase I digestion kit (QIAGEN). cDNA was synthesized using the Prime Script RT reagent kit (Takara Bio). Quantitative polymerase chain reaction analysis was carried out with a Light Cycler 480 (Roche Diagnostics) using SYBR Green I (Takara Bio) with 40 cycles of 5 seconds at 95°C, 15 seconds at 60°C, and 10 seconds at 72°C. Primer sequences used in this study are as follows: *mDia1,* 5′-CGA CGG CGG CAA ACA TAA G-3′ (forward) and 5′-TGC AGA GGA GTT TCT ATG AGC A-3′ (reverse); *mDia2*, 5′-GAG AAG CGA CCC AAG TTG CAT-3′ (forward) and 5′-GAA GGG GAG GTC TCT CTT TCT T-3′ (reverse); *mDia3*, 5′-AAT CTT CTG GAA GCC CTA CAG T-3′ (forward) and 5′-GGC CGT CTG TTA TCT GGA TTT C-3′ (reverse); *Gapdh*, 5′-AAA CCC ATC ACC ATC TTC CA-3′ (forward) and 5′-GTG GTT CAC ACC CAT CAC AA-3′ (reverse). The reaction protocol included preincubation at 95°C to activate FastStart DNA polymerase for 1 minute, 40 cycles of amplification each consisting of 5 seconds at 95°C, annealing for 15 seconds at 60°C, and elongation for 10 seconds at 72°C. Relative quantification was performed after determining the cycle threshold (C_t) values for reference gene *Gapdh*, and target genes in each sample sets according to the $2-\Delta\Delta C_t$ method.[24] We verified that all primer sets used in this study showed similar amplification efficiency. For each sample, triplicate test reactions and a control reaction lacking reverse transcriptase were used.

Statistical analysis

Unless otherwise indicated, data are presented as mean plus or minus SD. *P* values were calculated with the 2-tailed Student *t* test after data were confirmed to meet the criteria of normal distribution and equal variance using Lilliefors test.

Results

mRNA expression of the mDia family in DCs

We examined expression of mRNA for the mDia isoforms in DCs through a quantitative reverse-transcribed polymerase chain reaction analysis. We prepared B6 and mDia1$^{-/-}$ BMDCs, epidermal Langerhans cells (LCs), dermal and splenic DCs, and $CD4^+$ T cells of B6 mice and found that transcripts encoding all 3 isoforms were detected in all DC populations (Figure 1). The expression levels of the mDia isoforms in BMDCs were not affected by the maturation stimulated by LPS. In BMDCs from mDia1$^{-/-}$ mice, mDia1 expression was not detected as expected; and interestingly, mDia2 mRNA levels were higher than those of WT mice.

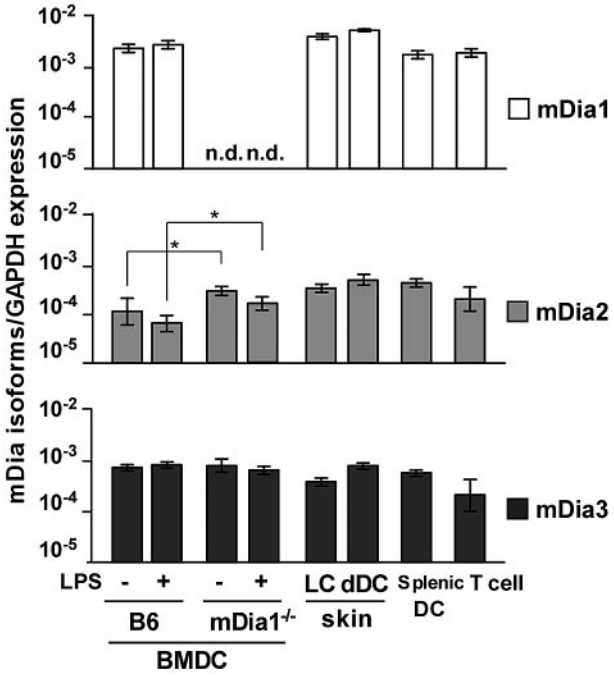

Figure 1. mRNA expression profiles of mDia isoforms in DCs. The mRNA expression profiles of mDia isoforms, mDia1, mDia2, and mDia3, in BMDCs from B6 and mDia1$^{-/-}$ mice stimulated with (+) or without (−) LPS, and LCs, dermal DCs, splenic DCs, and $CD4^+$ T cells from B6 mice. Data are expressed as the amounts of mRNA relative to that of glyceraldehyde-3-phosphate dehydrogenase (GAPDH). Data are mean ± SD (n = 3) of 3 independent experiments. n.d. indicates not dectected. *$P < .05$ vs corresponding B6 mice.

Impaired interstitial migration of cutaneous DCs in mDia1$^{-/-}$ mice

Initially, we evaluated the role of mDia1 in the development of DCs. The numbers of skin-derived DCs, resident DC subsets, splenic DC subsets, and skin DC subsets, and the maturation status of DCs in skin-draining LNs were comparable between B6 and mDia1$^{-/-}$ mice (supplemental Figure 1, available on the *Blood* Web site; see the Supplemental Materials link at the top of the online article). In addition, the number and maturation rates of mDia1$^{-/-}$ BMDCs were similar to those of B6 BMDCs in the absence (supplemental Figure 2A-D) or presence (supplemental Figure 2E) of 200 ng/mL LPS for the last 2 hours of 5-day cultivation period. These results suggest that mDia1 deficiency does not affect the development and maturation of conventional DCs.

We evaluated the significance of mDia1 with regard to DC functions in vivo. We used FITC, a fluorescent hapten, to induce DC maturation and mobilization.[25,26] FITC applied topically to the footpads of mice is taken up by cutaneous DCs, which then migrate to draining popliteal and inguinal LNs as MHC class II^+ $FITC^+$ cells.[27] The number of MHC class II^+ $FITC^+$ DCs that accumulated in draining LNs was significantly lower in mDia1$^{-/-}$ mice than in B6 mice (Figure 2A), and the numbers of $Langerin^+$ DCs (including both LCs and $Langerin^+$ dermal DCs) and $Langerin^-$

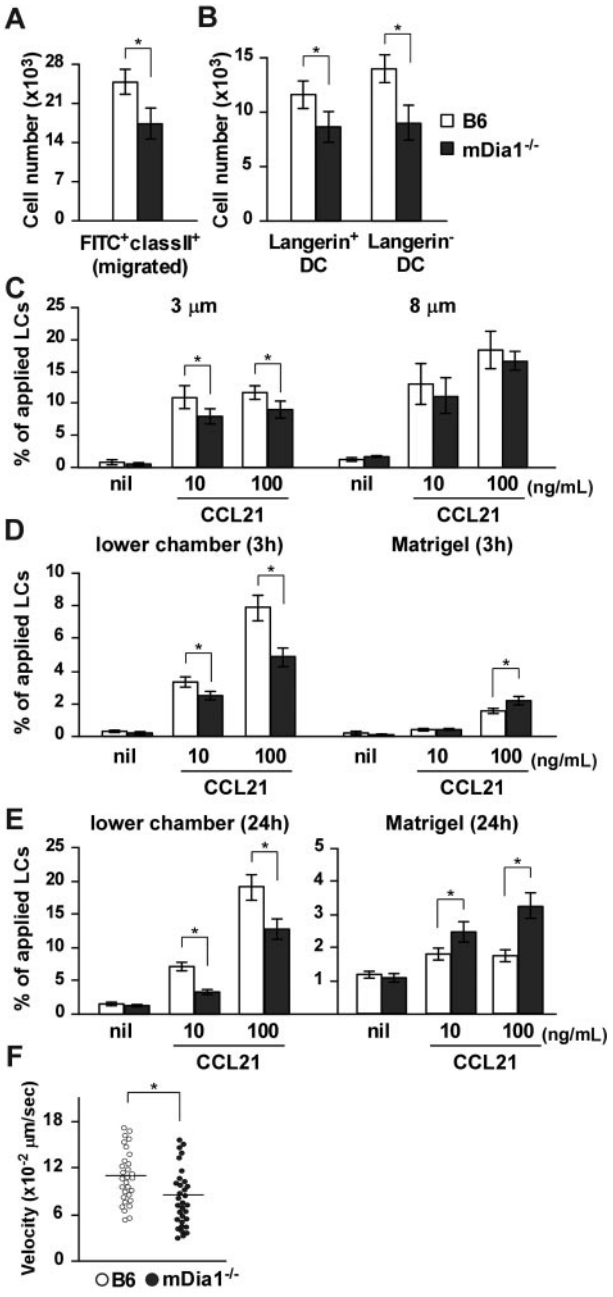

Figure 2. Impaired cutaneous DC migration in mDia1$^{-/-}$ mice. (A) The number of cutaneous DCs migrating from the skin to draining LNs. The numbers of FITC$^+$ MHC class II$^+$ total DCs (A) and FITC$^+$ MHC class II$^+$ Langerin$^+$ DC and FITC$^+$ MHC class II$^+$ Langerin$^-$ DC subsets (B) in draining LNs of B6 (open bars) and mDia1$^{-/-}$ mice (shaded bars) were analyzed 72 hours after application of FITC to the footpad. Bars represent the mean ± SD from at least 3 mice per group. (C) Mobility of LCs to CCL21. Epidermal cell suspensions were applied to the upper chamber of a transwell with 3 μm (left panel) and 8 μm (right panel) pore size without coating for 3 hours. Percentages of MHC class II$^+$ LCs that migrated from the upper chambers to the lower are shown. (D-E) Invasive movement of LCs to CCL21. Epidermal cell suspensions were applied to the upper chamber of a transwell coated with Matrigel for 3 hours (D) and 24 hours (E). The numbers of MHC class II$^+$ cells in the lower chamber (left panels) or in the Matrigel (right panels) were counted with flow cytometry. Data are mean ± SD of 3 independent experiments. *$P < .05$ vs corresponding B6 mice. (F) TAXIScan assay. BMDCs chemotaxing under the CCL21 gradient were analyzed with TAXIScan. BMDCs from B6 and mDia1$^{-/-}$ mice were compared in terms of the velocity. Data are mean ± SD of 4 independent experiments. *$P < .05$ vs corresponding B6 mice.

dermal DCs among the FITC$^+$ population of mDia1$^{-/-}$ mice were lower in mDia1$^{-/-}$ mice than in B6 mice (Figure 2B). On the other hand, FITC$^+$ mDia1$^{-/-}$ DCs were localized appropriately in the T zone of draining LNs, as observed using fluorescent microscopy (data not shown).

To assess the role of mDia1 in DC mobility, we performed a transwell assay with 3- and 8-μm pore sizes. Epidermal cell suspensions from the ears of B6 and mDia1$^{-/-}$ mice were applied to the upper transwell chambers, and the numbers of MHC class II$^+$ LCs in lower chambers with or without CCL21 were measured. The chemotaxis of mDia1$^{-/-}$ LCs to lower chambers containing CCL21 through the 8-μm transwell tended to be low, but not significantly so, compared with that of B6 LCs (Figure 2C right panel). The impaired chemotaxis of LCs by mDia1 deficiency became more distinct when transwells with a smaller pore size (3 μm) were used (Figure 2C left panel), suggesting that mDia1 is more essential to cell polarity-dependent transmigration. Next, we evaluated the invasion and directional movement of LCs by coating the polycarbonate filters of the 8-μm transwell with Matrigel.[28] Three hours after application, the number of LCs in the Matrigel was increased by the addition of CCL21 to the lower chamber, which was further increased by deficiency of mDia1 (Figure 2D right panel). On the other hand, the number of LCs in the lower chamber was decreased by deficiency of mDia1 (Figure 2D left panel). Similar results were obtained 24 hours after the chemotaxis assay (Figure 2E). These results suggest that mDia1 in DCs is indispensable for migration into the extracellular matrix protein-enriched area. We further evaluated the directional migration of BMDCs using TAXIScan and found that migration toward a gradient of the chemokine CCL21 was impaired by mDia1 deficiency in BMDCs (Figure 2F).

DC adhesion to FN was partially impaired by mDia1 deficiency

The interaction of DCs with extracellular matrix proteins, such as FN, is essential for their migration and formation of adhesion with integrins.[29] We evaluated localization of mDia1 in DCs and the effect of the deficiency of mDia1 on morphology and adhesions of BMDCs. We incubated BMDCs on plates coated with FN for 30 minutes and stained them with Alexa Fluor 488–labeled phalloidin and nonconjugated mDia1 Ab, followed by Alexa Fluor 546 goat anti–mouse IgG. Microscopic examination revealed that endogenous mDia1 was localized in the cytoplasm diffusely, and around the leading edge of B6 BMDCs strongly, and this localization was abolished in mDia1$^{-/-}$ BMDCs (Figure 3A).

We then evaluated the morphology and adhesion of BMDCs. We incubated BMDCs for 30 minutes, 4 hours, and 18 hours, and stained them with Alexa Fluor 488–labeled phalloidin and nonconjugated mDia1 Ab, followed by Alexa Fluor 546 goat anti–mouse IgG. Most B6 DCs exhibited membrane protrusions at 30 minutes after incubation. The cells spread out 4 hours after incubation, and stress fibers were clearly formed 18 hours after cultivation (Figure 3B). In contrast, almost all mDia1$^{-/-}$ BMDCs maintained their round shape without the formation of distinct membrane protrusions, but with distinct filopodia formation 30 minutes after incubation; and this apparent filopodia formation was still visible 4 hours, and even 18 hours after incubation (Figure 3B). To further evaluate podosome/focal adhesion formation, BMDCs were stained with Alexa Fluor 488–labeled phalloidin and nonconjugated vinculin Ab 4 hours after incubation, followed by Alexa Fluor 546 goat anti–mouse IgG. Although adhesion structures were detected in both B6 BMDCs and mDia1$^{-/-}$ BMDCs (supplemental Figure 3A), the frequencies of cells with podosome and focal adhesion formation were significantly lower in mDia1-deficient cells (podosome formation: 61.3% ± 4.3% vs 52.9% ± 2.6%; focal adhesion:

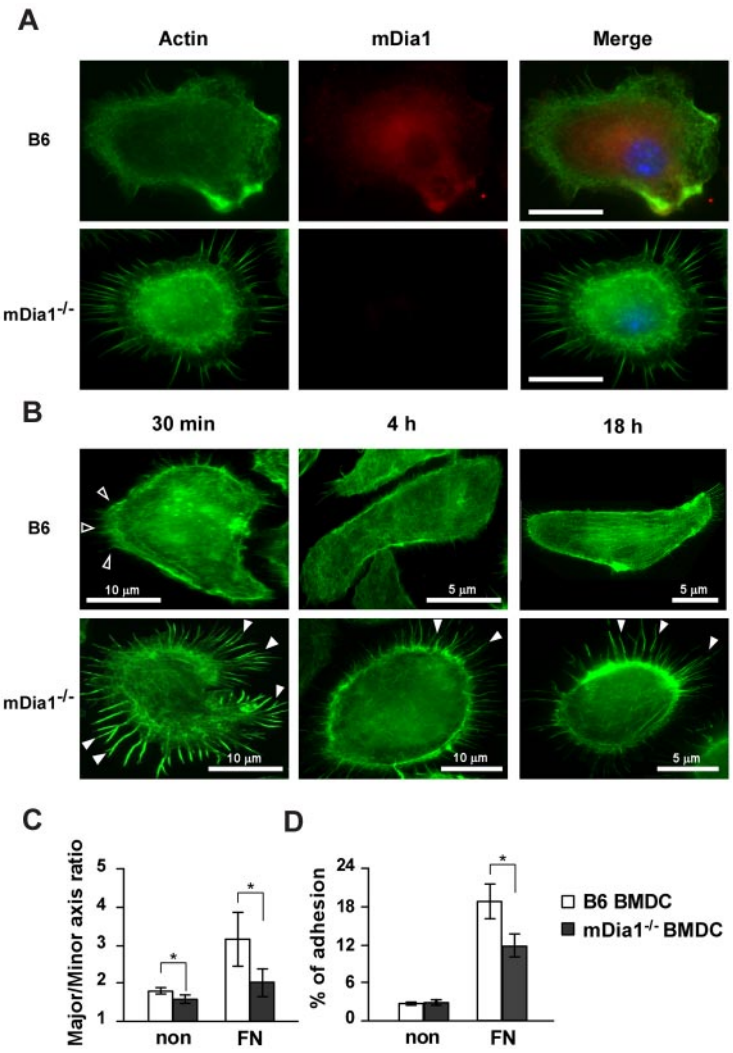

Figure 3. mDia localization in DCs and characterization of cell morphology and adhesion in mDia1$^{-/-}$ BMDCs. (A) mDia1 expression in DCs. B6 and mDia1$^{-/-}$ BMDCs were incubated on FN-coated coverslips for 16 hours and stained with phalloidin and mDia1 Ab to reveal F-actin (green) and mDia1 (red). The cell nucleus was detected using 4,6-diamidino-2-phenylindole staining (blue). Bar represents 10 μm. (B) B6 and mDia1$^{-/-}$ BMDCs incubated on FN-coated coverslips for 30 minutes, 4 hours, and 18 hours were stained with phalloidin; immunofluorescent images are shown. Open and closed arrowheads indicate membrane protrusion/lamellipodia and filopodia, respectively. (C) Morphology of BMDCs. B6 and mDia1$^{-/-}$BMDCs were incubated on coverslips coated with or without FN for 18 hours, and the major/minor axis ratio of BMDCs was measured. (D) Cell adhesion. B6 and mDia1$^{-/-}$ BMDCs were labeled with CFSE and incubated in a 96-well-plate coated with or without FN for 45 minutes. The percentage of adherent BMDCs was measured using a fluorometer. Data are mean ± SD of 3 independent experiments. *$P < .05$ vs corresponding B6 mice.

62.9% ± 3.1% vs 44.1% ± 3.1%; for B6 vs mDia1$^{-/-}$ BMDCs, respectively; data presented as average ± SEM from 5 independent experiments, with 20 cells from each group evaluated). We then examined the surface expression levels of integrins and adhesion molecules, such as CD11a (LFA-1), CD11c, CD54 (ICAM-1), CD62L (L-selectin), and CD11b, and found that expression levels of these molecules were comparable between B6 BMDCs and mDia1$^{-/-}$ BMDCs (supplemental Figure 3B). Lastly, we evaluated the cell polarity of BMDCs exposed for 30 minutes to CCL21 chemokine by staining with F-actin (supplemental Figure 3C). A chemokine gradient induced cell spreading of both B6 and mDia1$^{-/-}$ BMDCs with a visible leading edge (supplemental Figure 3C). We evaluated the cell polarity and cell spreading by scoring BMDCs for polarized accumulation of actin[30] and evaluated the major/minor axis ratio. Both the cell polarity and cell spreading of mDia1$^{-/-}$ BMDCs were less prominent than those of B6 BMDCs (supplemental Figure 3D-E). These results were consistent with the previous finding that the mean velocity of BMDCs to CCL21 was partially attenuated by mDia1 deficiency in a TAXIScan assay (Figure 2F).

We further evaluated the major/minor axes of BMDCs as indicators of cell polarity and protrusion after the BMDCs had been incubated on the coverslips for 16 hours. This parameter was significantly lower in mDia1$^{-/-}$ BMDCs than in B6 BMDCs (Figure 3C). We next assessed the adhesion of BMDCs after a 45-minute incubation period. The incidence of adhesion of BMDCs to the plates, indicated as a percentage, was higher when the plate was coated with FN, and the incidence of adhesion was significantly higher in B6 BMDCs than in mDia1$^{-/-}$ BMDCs (Figure 3D). These results suggest that mDia1 is an essential factor for the adhesion of DCs to FN, as well as for the establishment of cell polarity.

mDia1 deficiency in DCs impairs DC interaction with T cells

T-cell activation and differentiation require sustained interaction with DCs via integrins.[5] To investigate whether mDia1 deficiency in DCs impairs their interaction with T cells, we performed 3-dimensional live-imaging of DCs using 2-photon microscopy. To avoid environmental interference resulting from mDia1 deficiency in cells other than DCs, experiments were conducted using B6 mice as recipients for the transfer of B6 and mDia1$^{-/-}$ BMDCs. The dynamics of DC behavior in draining popliteal LNs were evaluated through the injection of CFSE- or CMTPX-labeled BMDCs pretreated with LPS into the footpads of B6 mice (supplemental Video 1). The mean velocities, turning angles (ie, deviations from the previous orientation), and displacements (ie, distances between starting and ending positions) were comparable between B6 DCs and mDia1$^{-/-}$ DCs (supplemental Figure 4A-C).

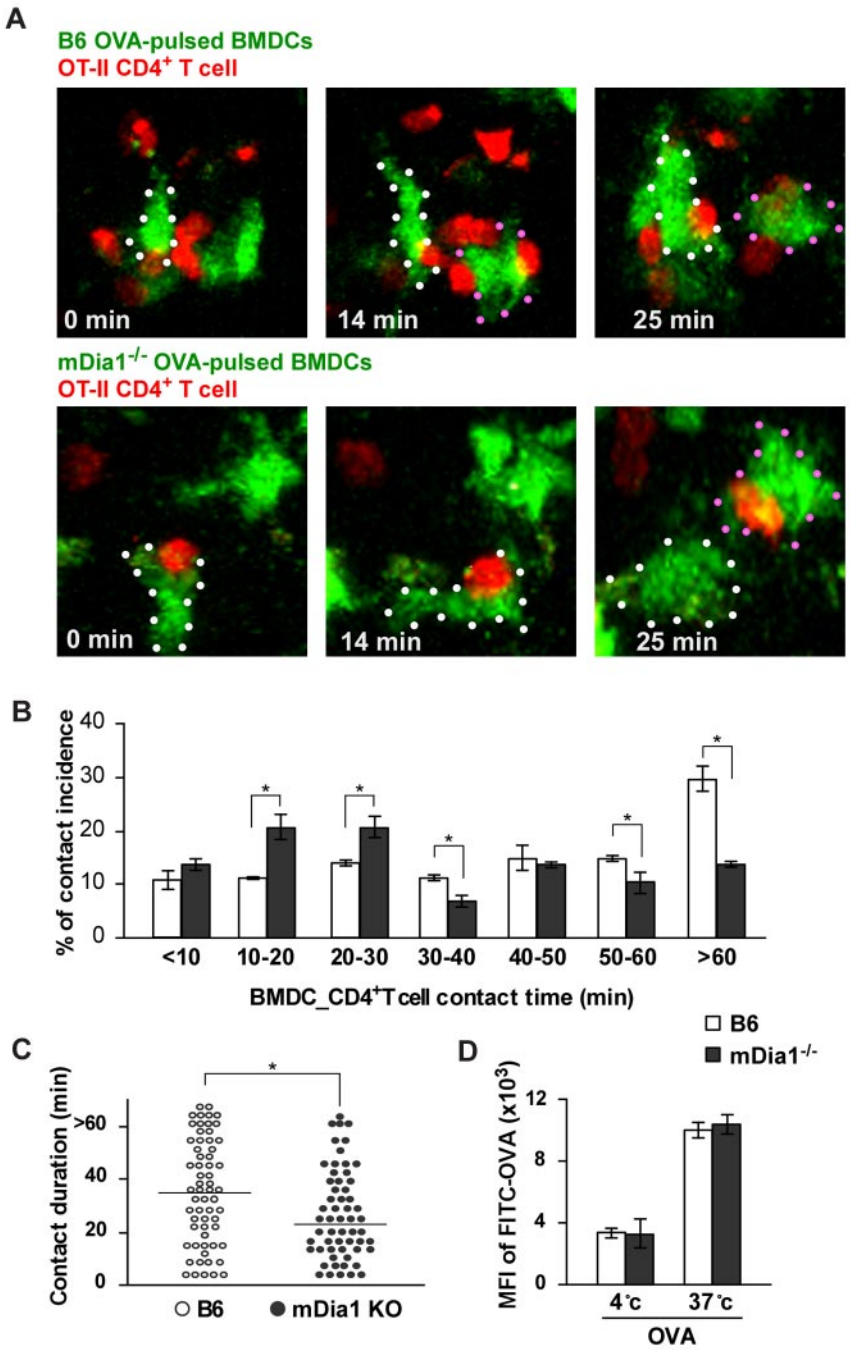

Figure 4. Impaired interaction with T cells resulting from mDia1 deficiency in DCs. (A) Time-lapse images of DC-T cell interaction ex vivo. OVA-pulsed CFSE-labeled B6 or mDia1$^{-/-}$ BMDCs were injected into mouse footpads, and CMTPX-labeled OT-II CD4^{+} T cells were intravenously administered. The popliteal LNs were collected and the DC–T-cell interaction was monitored using 2-photon microscopy; typical images at 0, 14, and 25 minutes are shown. White and red dots represent DCs. (B) Incidence of contact. Incidence of interactions of various durations between BMDCs and OT-II CD4^{+} T cells at 10-minute intervals. Data are mean ± SD and are representative of 3 experiments. (C) The overall duration of DC–T-cell interaction is shown. Data points represent individual durations. *$P < .05$ vs corresponding B6 mice. (D) Temperature-dependent activity of acquired antigens with FITC-OVA in MHC class II^{+} DCs of B6 mice and mDia1$^{-/-}$ mice. The activities of acquired antigens of DCs were observed by measuring the mean fluorescence intensity of ingested FITC at 4°C and 37°C for 45 minutes. Data are mean ± SD and are representative of 3 experiments.

We next evaluated DC–T-cell interaction in the LNs. T cells slow down their active migration and interact with DCs for up to several hours during the initial phase of T-cell priming.[31,32] BMDCs from B6 and mDia1$^{-/-}$ mice were pulsed with or without OVA, pretreated with LPS, labeled with CFSE, and injected into the footpads of mice. Twenty-four hours later, we intravenously transferred CMTPX-labeled CD4^{+} OT-II T cells, whose T-cell receptors specifically recognize OVA. An additional 2 hours later, we measured the duration of contacts formed between DCs and T cells in popliteal LNs during a 90-minute period of observation using 2-photon microscopy (supplemental Videos 2-3). The addition of OVA induced long-lasting contacts between B6 DCs and OT-II T cells; the length of these contacts was attenuated by mDia1 deficiency in DCs (Figure 4A-B). Our measurement of the durations of DC–T-cell conjugations revealed that mDia1$^{-/-}$ DCs exhibited higher rates of shorter-duration contacts, but lower rates of longer-duration contacts, than B6 DCs did (Figure 4B). Consistent with this, the overall mean duration of individual DC–T-cell interactions was shorter in mDia1$^{-/-}$ DCs than in B6 DCs (Figure 4C). We also evaluated whether the impaired T-cell–DC interaction brought about by mDia1 deficiency was not merely the result of impaired antigen acquisition by mDia1 BMDCs. The activity of temperature-dependent antigen acquisition of DCs was assessed by measuring FITC-labeled OVA in the cells using flow cytometry, and it was found that the activity levels were comparable between B6 and mDia1$^{-/-}$ mice (Figure 4D). Taken together, these results indicate that mDia1 expression in DCs is required to maintain sustained interactions with T cells.

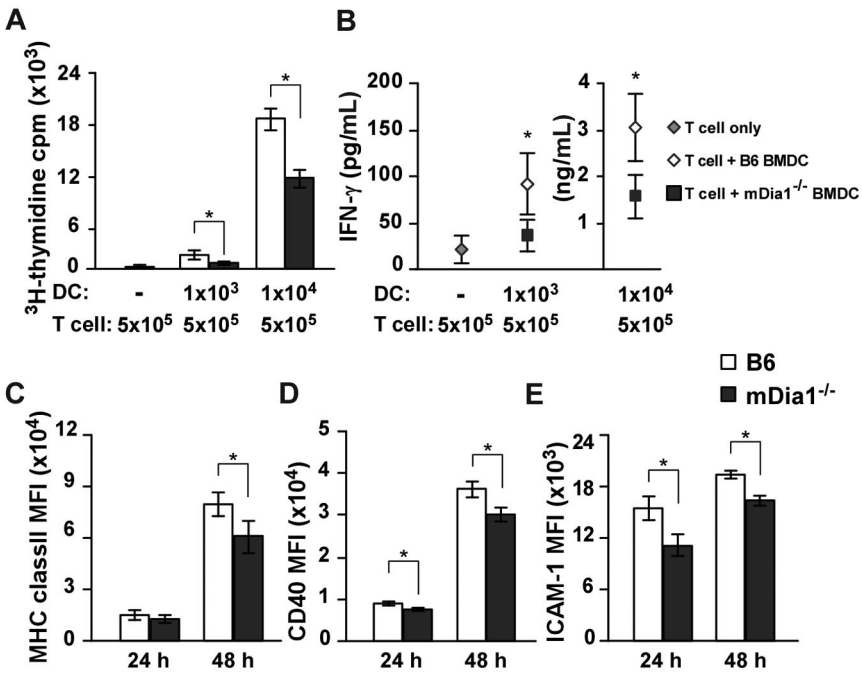

Figure 5. Impaired T cell-stimulatory capacity of DCs resulting from mDia1 deficiency. (A-B) Alloreactive CD4$^+$ T cells were purified from BALB/c mice and stimulated with or without B6 or mDia1$^{-/-}$ BMDCs in 200 μL of cRPMI for 72 hours. The numbers of each cell subset are shown in the figure. ^{3}H-Thymidine incorporation in triplicate wells as an indicator of T-cell proliferation (A) and levels of IFN-γ in the culture supernatant (B) were measured. (C-E) The expression levels of MHC class II (C), CD40 (D), and CD54 (ICAM-1) (E) of BMDCs at 24 hours and 48 hours. Data are mean ± SD and are representative of 3 independent experiments. *$P < .05$ vs corresponding B6 mice.

mDia1 deficiency attenuates T cell-stimulatory capacity of DCs in vitro

Based on the results we had thus far obtained, we sought to clarify whether mDia1 deficiency in DCs attenuated T cell-stimulatory capacity by MLR. Alloreactive CD4$^+$ T cells were purified from BALB/c mice and stimulated with B6 or mDia1$^{-/-}$ BMDCs. Proliferation of T cells was lower in response to stimulation with mDia1$^{-/-}$ BMDCs than in response to stimulation with B6 BMDCs (Figure 5A). Consistently, levels of interferon-γ (IFN-γ) were lower in the supernatants of T-cell cultures stimulated with mDia1$^{-/-}$ BMDCs than in those stimulated with B6 BMDCs (Figure 5B). We further examined the expression levels of MHC class II, CD40, and CD54 as indicators of DC maturation 24 and 48 hours after cultivation, and found that mean fluorescence intensities of all surface markers of mDia1$^{-/-}$ BMDCs were lower than those of B6 BMDCs 48 hours after cultivation (Figure 5C-E). We assume that DCs undergo a further maturation on sustained interaction with T cells in an mDia1-dependent manner; therefore, mDia1 deficiency in DCs leads to impaired T-cell–stimulatory capacity in MLR.

Priming of T cells is reduced by mDia1 deficiency in vivo

Based on these results, we hypothesized that mDia1 deficiency in DCs leads to the attenuation of T-cell priming in vivo. We immunized B6 and mDia1$^{-/-}$ mice with OVA emulsified in CFA and transferred CFSE-labeled OT-II CD4$^+$ T cells intravenously. Forty-eight hours later, draining popliteal and inguinal LN cells were dissociated, and dividing cells were measured with flow cytometry (Figure 6A-B). The numbers of total and dividing OT-II CD4$^+$ T cells per draining LNs were significantly attenuated in mDia1$^{-/-}$ mice compared with B6 mice (Figure 6C). We also examined nondraining axillary LN cells for comparison purposes and found that the frequencies of CFSE$^+$ OT-II CD4$^+$ T cells to total cells were comparable in mDia1$^{-/-}$ and B6 mice (supplemental Figure 5). Cells in the process of division were not detected (supplemental Figure 5). In addition, the numbers of activated CD69$^+$ CFSE$^+$ cells and the relative amounts of IFN-γ mRNA were lower in the draining LNs of mDia1$^{-/-}$ mice than in those of B6 mice (Figure 6D-E).

We next repeated the experiments using OT-I CD8$^+$ T cells instead of OT-II CD4$^+$ T cells, to evaluate the capacity of DCs to stimulate CD8$^+$ T cells. Like that of OT-II CD4$^+$ T cells, stimulation of OT-I CD8 T-cell proliferation was impaired by mDia1 deficiency in DCs (Figure 6F). These findings indicate that DCs require mDia1 to prime both CD4$^+$ and CD8$^+$ T cells in vivo.

Finally, we evaluated the impact of mDia1 deficiency in DCs on immune responses using a DTH model. B6 and mDia1$^{-/-}$ mice were subcutaneously sensitized with OVA in CFA in the front footpads and challenged with OVA in CFA in the hind footpads. Mice not subjected to OVA sensitization were used as a negative control. The hind footpad swelling change during the 48 hours after challenge was attenuated in mDia1$^{-/-}$ mice compared with B6 mice (Figure 6G), providing further evidence that mDia1 is critical for the T-cell priming ability of DCs in vivo. To avoid environmental interference resulting from mDia1 deficiency in cells other than DCs, we transferred B6 or mDia1$^{-/-}$ BMDCs pulsed with OVA into the front footpads and challenged the mice with OVA in CFA into the hind footpads. Mice injected with B6 BMDCs that had not been pulsed with OVA during sensitization were used as a negative control. The footpad thickness change was almost entirely abolished by mDia1 deficiency in DCs (Figure 6H). Thus, mDia1 in DCs is critical for the initiation of DTH response via T-cell priming in vivo.

Discussion

The role of mDia1 in the reorganization of the DC cytoskeleton has not yet been fully studied. In this report, we demonstrated that the number and maturation of DC subsets in the LNs, spleen, and the skin in the steady state, the development and maturation of BMDCs in vitro, and the motility of BMDCs in the LNs were not affected by mDia1 deficiency. However, DCs from mDia1$^{-/-}$ mice exhibited impaired transmigration of LCs through transwells with small pore

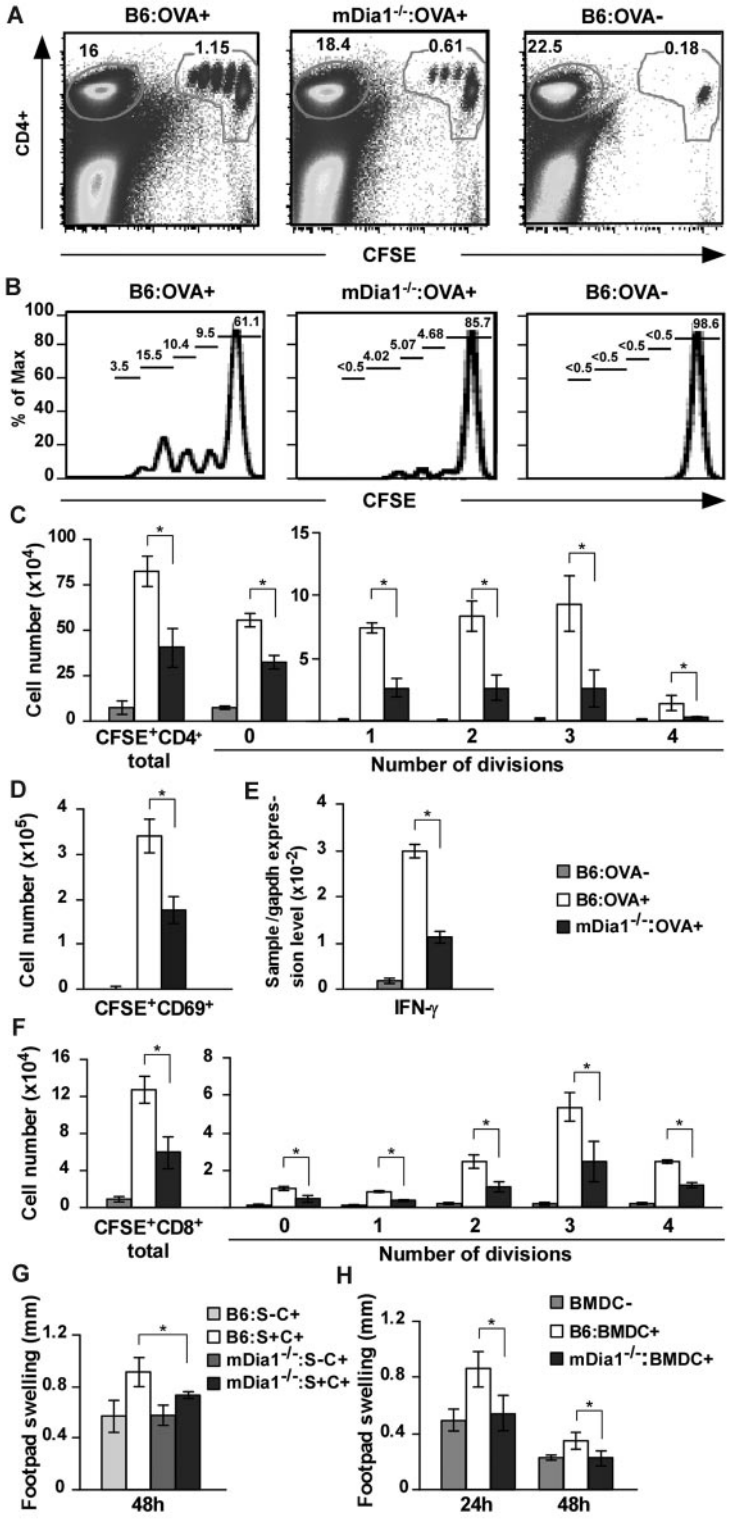

Figure 6. Attenuated CD4$^+$ and CD8$^+$ T-cell stimulation in mDia1$^{-/-}$ BMDCs. (A-D) OT-II CD4$^+$ T-cell stimulation by DCs. B6 and mDia1$^{-/-}$ mice were injected with CFA in the presence or absence of OVA, and CFSE-labeled OT-II CD4$^+$ T cells were transferred intravenously. Forty-eight hours later, skin-draining popliteal and inguinal LN cells were collected and stained with CD4. Flow cytometry profiles (A), histograms of CFSE$^+$ CD4$^+$ cells (B), the numbers of CD4$^+$ T cells per draining LNs in each division (C), and the numbers of CD69$^+$ activated T cells (D) per draining LNs are shown. The numbers indicated in A are the ratio (%) of CD4$^+$ CFSE$^+$ cells (right) and CD4$^+$ CFSE$^-$ cells to total cells. The numbers indicated in panel B are the ratio of each fraction to CD4$^+$ CFSE$^+$ cells. (E) IFN-γ mRNA expression was evaluated through quantitative reverse-transcribed polymerase chain reaction analysis. (F) OT-I CD8$^+$ T-cell stimulation by DCs. CFSE-labeled OT-I CD8$^+$ T cells were transferred intravenously to mice that had been pretreated as described in panels A to E, and the distribution of cell numbers in draining LNs is shown. (G) DTH induced by injection with OVA plus CFA. B6 and mDia1$^{-/-}$ mice were sensitized with OVA in CFA subcutaneously at the front footpads and challenged with OVA in CFA in the hind footpads. B6 and mDia1$^{-/-}$ mice that had not received OVA sensitization were used as negative controls. Footpad thickness change over 48 hours is shown. S indicates sensitization; and C, challenge. (H) DTH induced by OVA-pulsed BMDCs. We injected B6 or mDia1$^{-/-}$ BMDCs pulsed with (BMDC$^+$) or without (BMDC$^-$) OVA into the front footpads and challenged the mice by injecting OVA in CFA into the hind footpads. Administration of B6 BMDCs not pulsed with OVA during sensitization was used as a negative control. Footpad swelling data over 24 hours and 48 hours after challenge with OVA in CFA are shown. Data are mean ± SD and are representative of 3 independent experiments with similar results.

size, directional migration toward a chemokine gradient, cell adhesion to FN, and interaction with T cells. Consistent with this, the CD4$^+$ and CD8$^+$ T-cell–stimulating capacity of DCs, as well as their OVA-induced DTH response in vivo, were attenuated as a result of mDia1 deficiency. The results herein demonstrate the involvement of mDia1 at each step of DC functioning, as well as the importance of actin cytoskeletal reorganization and cognate interaction through mDia1 in DCs.

Cell migration is frequently described as a multistep cycle. F-actin polymerization at the cell surface induces a membrane protrusion, which is subsequently anchored to the extracellular matrix by integrins, which couple with the cytoskeleton and transduce the internal force via the actin cytoskeletal network.[33,34] Although motility in the LNs and invasion into the extracellular matrix–rich area remained mostly intact in mDia1$^{-/-}$ BMDCs, the transmigration to CCL21 through transwells with small pore size,

migration of mDia1$^{-/-}$ BMDCs across the Matrigel-coated transwell, and directional migration to chemokine on TAXIScan were all impaired. In addition, cell spreading and membrane protrusion were attenuated in mDia1$^{-/-}$ BMDCs. These findings probably explain the in vivo finding that FITC-induced cutaneous DC migration from the skin to the draining LNs was impaired. Using rat C6 glioma cells, Yamana et al demonstrated that mDia1 is required for cell polarization, cell focal adhesion turnover, and microtubule stabilization, possibly through the collaboration with Rac and Cdc42.[14] Therefore, the role of Rac/Cdc42 in mDia1$^{-/-}$ DCs in cell spreading and adhesion is worthy of future study.

Recent findings have suggested that integrins are essential for crossing the endothelial or epithelial lining, but not for migration of DCs in 3-dimensional environments.[35] Instead, these cells migrate solely by the force of actin-network expansion, which promotes the protrusive flow of the leading edge. In addition, the dynamics of DC behavior were not affected by deficiency of mDia1 in LNs in the steady state, which implies that mDia1 is not necessary for DCs to perform "amoeboid movement."[36] On the other hand, the invasive migration through the Matrigel and the directional migration to a chemokine gradient were attenuated in mDia1$^{-/-}$ BMDCs. Therefore, mDia1 appears indispensable for invasive movement in the extracellular matrix-rich area and directional movements toward a chemokine gradient, which depends on cell polarity (at least in part).

It is notable that behavior similar to that of mDia1$^{-/-}$ DCs, such as decreased adhesion and defects in T cell-stimulating capacity, has been observed in WASP$^{-/-}$ DCs.[37-39] Yet the impairments in maturation and chemotaxis and the dislocalization of DCs in the LNs that were observed in WASP$^{-/-}$ DCs[38] were not observed in mDia1$^{-/-}$ DCs. Yet although WASP-deficient DCs form abnormal lamellipodia resulting in hyperelongated morphology,[40] mDia1$^{-/-}$ DCs exhibit a rather round morphology without stress fiber formation. Collectively, these results suggest that the 2 actin-nucleating systems work together to enable the functions of DCs and that the lack of either cannot be compensated for by the other.

Given that the mDia family plays an elemental role in the actin filament dynamics in DCs, it is surprising that mDia1$^{-/-}$ DCs exhibited relatively mild and limited dysfunction. We[16] and others[17] have previously found only partial impairment of T-cell trafficking in mDia1$^{-/-}$ mice. This may be partly explained by the fact that the roles of the other mDia isoforms, mDia2 and mDia3, overlap somewhat with those of mDia1.[9] In addition, we demonstrated that the mDia2 expression level in mDia1$^{-/-}$ DCs was elevated, which suggests that mDia2 might be induced to compensate for the deficiency of mDia1. Intriguingly, although mDia1 deficiency appears to cause only partial impairment of DC functioning at each step, its overall impact on the DTH response in DCs was nearly complete. The roles of mDia2 and mDia3 in DCs, as well as the role of WASP in relation to mDia1, are important topics for future study.

Acknowledgments

The authors thank Dr Yuji Kamioka and Dr Michiyuki Matsuda for their technical assistance and advice.

This work was supported in part by Scientific Research from the Ministry of Education, Culture, Sports, Science and Technology and the Ministry of Health, Labor, and Welfare of Japan (Grants-in-Aid).

Authorship

Contribution: H.T. performed experiments, analyzed data, and wrote the paper; G.E., K.I., T.H., S. Nakajima, C.S.M., A.O., T.I., M.T., T.W., Y.M., S. Narumiya, and T.O. analyzed and discussed the data; and K.K. designed the research, analyzed the data, and cowrote the paper.

Conflict-of-interest disclosure: The authors declare no competing financial interests.

Correspondence: Kenji Kabashima, Department of Dermatology, Kyoto University Graduate School of Medicine, Yoshida, Sakyo-ku, Kyoto 606-8501, Japan; e-mail: kaba@kuhp.kyoto-u.ac.jp.

References

1. Banchereau J, Steinman RM. Dendritic cells and the control of immunity. *Nature.* 1998;392(6673):245-252.
2. Alvarez D, Vollmann EH, von Andrian UH. Mechanisms and consequences of dendritic cell migration. *Immunity.* 2008;29(3):325-342.
3. Randolph GJ, Angeli V, Swartz MA. Dendritic-cell trafficking to lymph nodes through lymphatic vessels. *Nat Rev Immunol.* 2005;5(8):617-628.
4. Kabashima K, Shiraishi N, Sugita K, et al. CXCL12-CXCR4 engagement is required for migration of cutaneous dendritic cells. *Am J Pathol.* 2007;171(4):1249-1257.
5. Dustin ML. T-cell activation through immunological synapses and kinapses. *Immunol Rev.* 2008;221:77-89.
6. Ridley AJ, Schwartz MA, Burridge K, et al. Cell migration: integrating signals from front to back. *Science.* 2003;302(5651):1704-1709.
7. Calle Y, Burns S, Thrasher AJ, Jones GE. The leukocyte podosome. *Eur J Cell Biol.* 2006;85(3):151-157.
8. Pulecio J, Tagliani E, Scholer A, et al. Expression of Wiskott-Aldrich syndrome protein in dendritic cells regulates synapse formation and activation of naive CD8+ T cells. *J Immunol.* 2008;181(2):1135-1142.
9. Faix J, Grosse R. Staying in shape with formins. *Dev Cell.* 2006;10(6):693-706.
10. Thrasher AJWA Sp in immune-system organization and function. *Nat Rev Immunol.* 2002;2(9):635-646.
11. Ochs HD, Thrasher AJ. The Wiskott-Aldrich syndrome. *J Allergy Clin Immunol.* 2006;117(4):725-738; quiz 739.
12. Le Clainche C, Carlier MF. Regulation of actin assembly associated with protrusion and adhesion in cell migration. *Physiol Rev.* 2008;88(2):489-513.
13. Goode BL, Eck MJ. Mechanism and function of formins in the control of actin assembly. *Annu Rev Biochem.* 2007;76:593-627.
14. Yamana N, Arakawa Y, Nishino T, et al. The Rho-mDia1 pathway regulates cell polarity and focal adhesion turnover in migrating cells through mobilizing Apc and c-Src. *Mol Cell Biol.* 2006;26(18):6844-6858.
15. Narumiya S, Tanji M, Ishizaki T. Rho signaling, ROCK and mDia1, in transformation, metastasis and invasion. *Cancer Metastasis Rev.* 2009;28(1):65-76.
16. Sakata D, Taniguchi H, Yasuda S, et al. Impaired T lymphocyte trafficking in mice deficient in an actin-nucleating protein, mDia1. *J Exp Med.* 2007;204(9):2031-2038.
17. Eisenmann KM, West RA, Hildebrand D, et al. T cell responses in mammalian diaphanous-related formin mDia1 knock-out mice. *J Biol Chem.* 2007;282(34):25152-25158.
18. Kobayashi M, Azuma E, Ido M, et al. A pivotal role of Rho GTPase in the regulation of morphology and function of dendritic cells. *J Immunol.* 2001;167(7):3585-3591.
19. Kabashima K, Murata T, Tanaka H, et al. Thromboxane A2 modulates interaction of dendritic cells and T cells and regulates acquired immunity. *Nat Immunol.* 2003;4(7):694-701.
20. Kabashima K, Sugita K, Shiraishi N, Tamamura H, Fujii N, Tokura Y. CXCR4 engagement promotes dendritic cell survival and maturation. *Biochem Biophys Res Commun.* 2007;361(4):1012-1016.
21. Yoshiki R, Kabashima K, Sugita K, Atarashi K, Shimauchi T, Tokura Y. IL-10-producing Langerhans cells and regulatory T cells are responsible for depressed contact hypersensitivity in grafted skin. *J Invest Dermatol.* 2009;129(3):705-713.
22. Nitta N, Tsuchiya T, Yamauchi A, Tamatani T, Kanegasaki S. Quantitative analysis of eosinophil chemotaxis tracked using a novel optical device: TAXIScan. *J Immunol Methods.* 2007;320(1):155-163.

23. Miller MJ, Wei SH, Parker I, Cahalan MD. Two-photon imaging of lymphocyte motility and antigen response in intact lymph node. *Science.* 2002;296(5574):1869-1873.

24. Livak KJ, Schmittgen TD. Analysis of relative gene expression data using real-time quantitative PCR and the 2(-Delta Delta C(T)) Method. *Methods.* 2001;25(4):402-408.

25. Randolph GJ, Inaba K, Robbiani DF, Steinman RM, Muller WA. Differentiation of phagocytic monocytes into lymph node dendritic cells in vivo. *Immunity.* 1999;11(6):753-761.

26. Sato K, Imai Y, Irimura T. Contribution of dermal macrophage trafficking in the sensitization phase of contact hypersensitivity. *J Immunol.* 1998; 161(12):6835-6844.

27. Kabashima K, Sakata D, Nagamachi M, Miyachi Y, Inaba K, Narumiya S. Prostaglandin E2-EP4 signaling initiates skin immune responses by promoting migration and maturation of Langerhans cells. *Nat Med.* 2003;9(6):744-749.

28. Sanz-Moreno V, Gadea G, Ahn J, et al. Rac activation and inactivation control plasticity of tumor cell movement. *Cell.* 2008;135(3):510-523.

29. Pankov R, Yamada KM. Fibronectin at a glance. *J Cell Sci.* 2002;115(20):3861-3863.

30. Shimonaka M, Katagiri K, Nakayama T, et al. Rap1 translates chemokine signals to integrin activation, cell polarization, and motility across vascular endothelium under flow. *J Cell Biol.* 2003;161(2):417-427.

31. Mempel TR, Henrickson SE, Von Andrian UH. T-cell priming by dendritic cells in lymph nodes occurs in three distinct phases. *Nature.* 2004;427 (6970):154-159.

32. Hugues S, Fetler L, Bonifaz L, Helft J, Amblard F, Amigorena S. Distinct T cell dynamics in lymph nodes during the induction of tolerance and immunity. *Nat Immunol.* 2004;5(12):1235-1242.

33. Lauffenburger DA, Horwitz AF. Cell migration: a physically integrated molecular process. *Cell.* 1996;84(3):359-369.

34. Mitchison TJ, Cramer LP. Actin-based cell motility and cell locomotion. *Cell.* 1996;84(3):371-379.

35. Lammermann T, Bader BL, Monkley SJ, et al. Rapid leukocyte migration by integrin-independent flowing and squeezing. *Nature.* 2008;453(7191):51-55.

36. de Bruyn PPH. The amoeboid movement of the mammalian leukocyte in tissue culture. *Ant. Rec.* 1946;95:117-192.

37. Bouma G, Burns S, Thrasher AJ. Impaired T-cell priming in vivo resulting from dysfunction of WASp-deficient dendritic cells. *Blood.* 2007; 110(13):4278-4284.

38. Bouma G, Burns SO, Thrasher AJ. Wiskott-Aldrich syndrome: immunodeficiency resulting from defective cell migration and impaired immunostimulatory activation. *Immunobiology.* 2009; 214(9):778-790.

39. de Noronha S, Hardy S, Sinclair J, et al. Impaired dendritic-cell homing in vivo in the absence of Wiskott-Aldrich syndrome protein. *Blood.* 2005; 105(4):1590-1597.

40. Burns S, Thrasher AJ, Blundell MP, Machesky L, Jones GE. Configuration of human dendritic cell cytoskeleton by Rho GTPases, the WAS protein, and differentiation. *Blood.* 2001;98(4):1142-1149.